

From chaotic to $1/f$ processes in solar mcw-bursts

V.B. Ryabov¹, A.V. Stepanov², P.V. Usik¹, D.M. Vavriv¹, V.V. Vinogradov¹, and Yu.F. Yurovsky²

¹ Institute of Radio Astronomy, 4 Krasnoznamennaya St., 310002 Kharkov, Ukraine

² Crimean Astrophysical Observatory, RT-22, Katziveli, Crimea, 334247 Ukraine

Received 10 April 1996 / Accepted 18 November 1996

Abstract. Solar bursts with superfine time structure observed at 2.5 and 2.85 GHz at the Crimean Astrophysical Observatory have been analyzed by means of statistical methods for nonlinear dynamical systems. Finite values of the correlation dimension have not been detected for all the studied events. The presence of a $1/f^\gamma$ component in many of the processed events has been found by means of wavelet analysis and maximum likelihood technique. The model of uncorrelated pulses is proposed as the one capable of producing a $1/f^\gamma$ shape of the power spectrum. A procedure is developed for extracting the parameters of pulse sequences from the data, and the magnitudes of pulse duration, amplitude, and repetition frequency are estimated for the solar burst events.

Key words: Sun: flares – Sun: radio radiation – chaos – data analysis

1. Introduction

Considerable recent attention has been focused on superfine time structure of solar microwave emission and, in particular, on irregular pulsations with typical time scale of the order of milliseconds (Slottje 1978; Dennis et al. 1987; Stepanov & Yurovsky 1990; Benz & Aschwanden 1991; Vlahos et al. 1983; Zaitsev et al. 1985; Aschwanden 1987; Isliker 1992, Barrow et al. 1994). About ten years ago the hypothesis has been put forward that the mechanism responsible for the formation of the irregular behavior may be of deterministic nature. In accordance with it, the complicated temporal structures in the solar emission detected in many observations have been suggested to be chaotic processes, with finite value of the associated correlation (fractal) dimension.

Preliminary reports (Kurths & Herzel 1987; Kurths & Karlicky 1989; Isliker 1992) were in favor of such a theory. However, more careful analysis (Isliker & Benz 1994) has revealed that in almost all the cases the detected finite value of correlation dimension was a spurious effect caused by intrinsic difficulties

in the calculation process. At the same time, the absence of a rigorous model for the emission mechanism does not permit one to generalize the already obtained results concerning the high dimensionality of dynamical processes in the solar corona to wave bands not yet investigated. On the other hand, it should be noted that any, even carefully checked, result revealing either deterministic or noise nature of the studied signal in itself does not allow one to understand in details the physics of the solar microwave emission and does not clarify the mechanism responsible for the generation of the millisecond pulsations. This fact requires alternative approaches to be used, together with the correlation dimension analysis.

In the present work the analysis is carried out of several solar radio bursts observed at the Crimean Astrophysical Observatory (CrAO) at 2.5 and 2.85 GHz with millisecond time resolution (sampling time $\Delta t_s \approx 8 - 10$ ms). To our knowledge, study of dynamic properties of the flare process has not been conducted before in this band.

As a first step in our study we calculate the correlation dimension ν , following the standard procedure of Takens, Grassberger and Procaccia. We introduce an error analysis of the calculated value of ν which permits us to control the accuracy and optimize the calculation procedure. We have demonstrated that in this particular wave band the investigated processes are either deterministic with the dimension at least greater than 10, or they are of stochastic origin. Hence, our results are in agreement with those reported in studies performed in different wave bands (Isliker & Benz 1994). In the following we develop the hypothesis that such processes are stochastic ones and, moreover, belong to the class of $1/f$ noise. We exploit the wavelet analysis together with the maximum likelihood statistical technique (Wornell & Oppenheim 1992) in order to detect the $1/f$ signal and separate it from the background noise. It has turned out that in many of the events under investigation a $1/f$ process was present with rather high intensity, compared to the background. The detected $1/f$ nature of the flare emission enables us to propose an interpretation of the millisecond temporal structure of the emission in terms of uncorrelated pulses. We estimate the characteristic time scale of an individual pulse and discuss possible physical mechanisms responsible for the generation of pulsed radiation.

Send offprint requests to: V.B. Ryabov

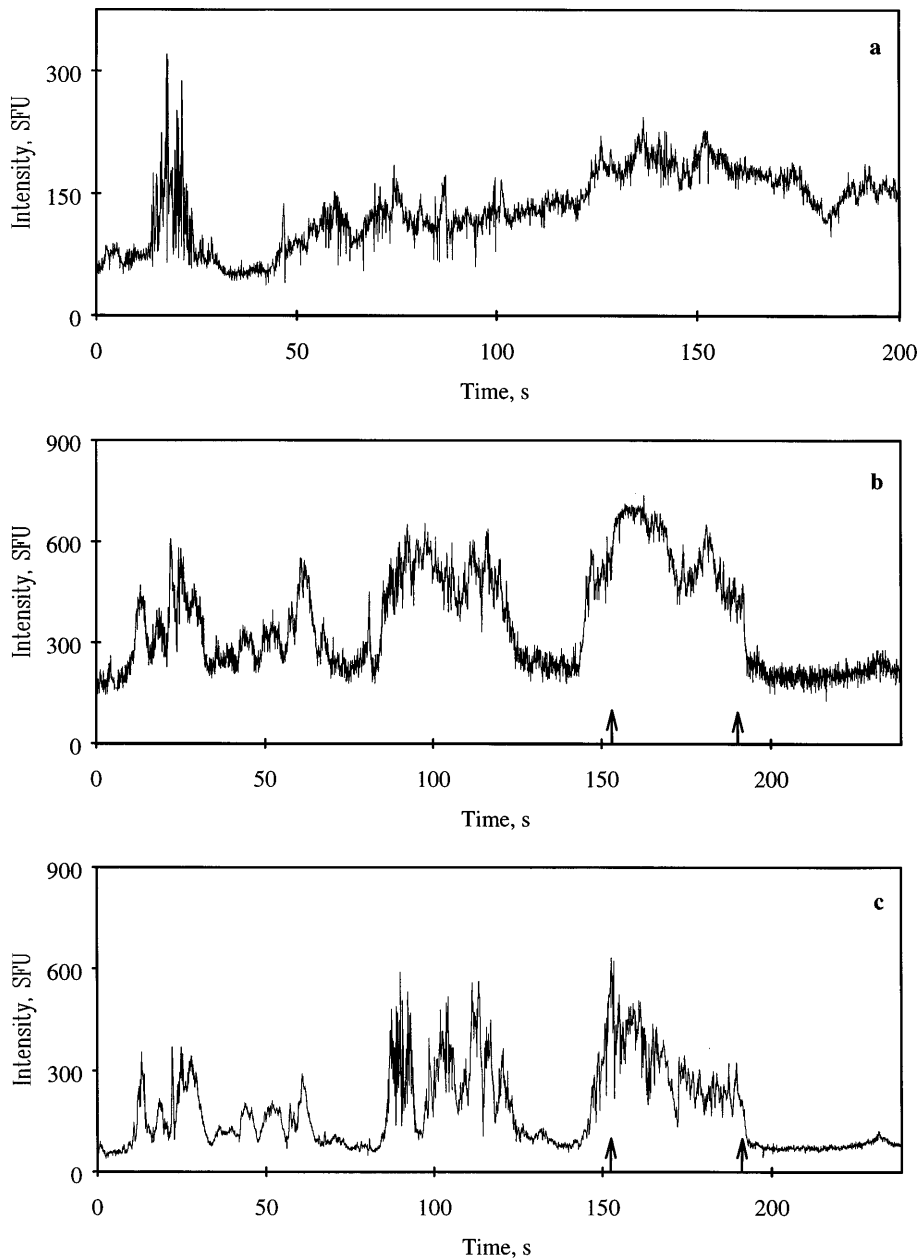


Fig. 1a–e. Time profiles of bursts: **a** 12th of March, 1989 at 2.85 GHz, **b** 17th of November 1991 at 2.5 GHz, **c, d, e** 17th of November 1991 at 2.85 GHz. The interval with a spurious finite value of dimension is marked by arrows.

The paper is organized as follows. Sect. 2 comprises the description of the experiment and observational data. In Sect. 3 the results of calculation of ν are given, with some discussion and interpretation. Sect. 4 presents the wavelet analysis of the data, and Sect. 5 contains the description of a possible scenario for the generation of millisecond pulses. Sect. 6 presents the discussion. Appendix A is devoted to the details of systematic and random errors in correlation dimension algorithm. In Appendix B we give a sketch of the procedure for detecting a $1/f$ signal on the white noise background and for evaluating the qualitative characteristics of the signal.

2. Observational data

The data analyzed below have been obtained with the radio telescope of CrAO which has the 3 m dish under a radio transparent

dome, at which the daily observations are performed in accordance with the Solar Service program at frequencies 2.5 and 2.85 GHz. The radiometer bandwidth is 40 MHz, and sensitivity is 6% of the quiet Sun radio emission flux. The millisecond-rate of recording is turned on automatically after detecting an increase of the radio emission flux by 5% of the preburst level.

We have processed the events whose characteristics are given in the Table 1. In Fig. 1a–c the time profiles of the bursts N1 and 5 (according to the Table numbering) are depicted as examples. The feature of both realizations is their essential non-stationarity which is known to hamper the investigations by both traditional methods of correlation or spectral analysis and techniques related to the dimension calculation.

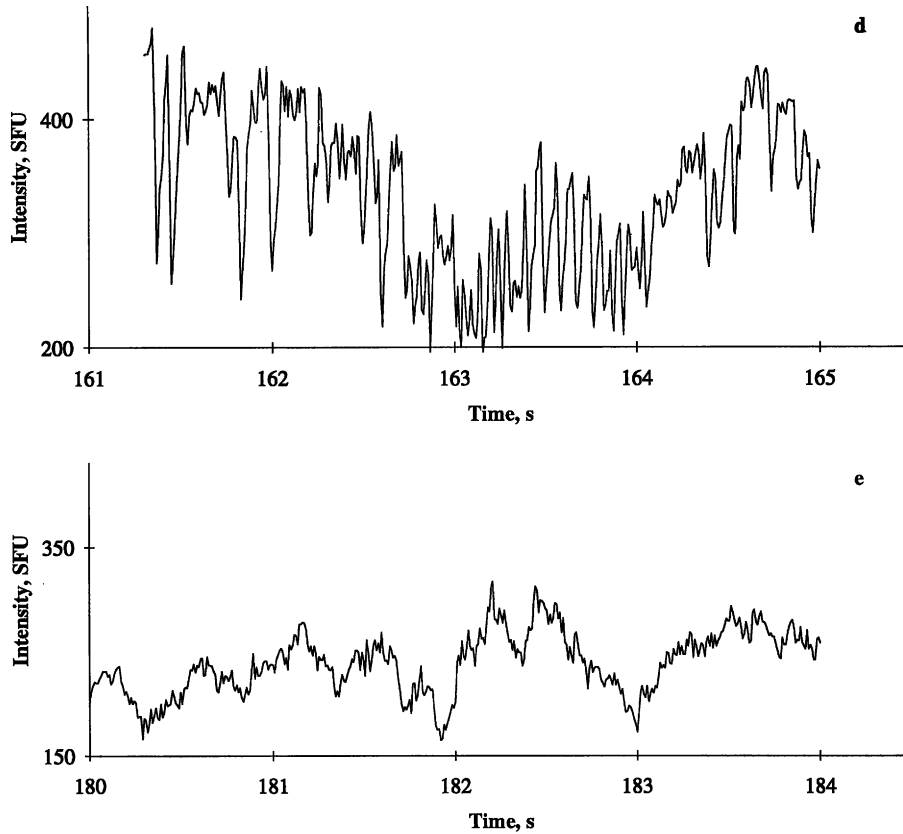


Fig. 1a–e. (Continued)

Table 1. List of events

No.	Date	Number of points	Frequency (GHz)	Start of fragment (UT)	End of fragment (UT)	Sampling frequency (Hz)
1	89/03/12	25000	2.85	08:17:36	08:20:50	125
2	89/09/01	12431	2.85	06:16:52	07:10:00	125
3	89/10/19	3125	2.85	12:48:34	13:15:00	115
4	90/02/12	4500	2.85	08:50:52	08:51:26	125
5	91/11/17	26387	2.5, 2.85	07:04:05	07:07:37	111
6	91/04/16	17400	2.5, 2.85	11:41:26	11:44:00	113
7	91/04/16	33400	2.5, 2.85	11:49:01	11:53:57	113

3. Correlation dimension analysis

We have calculated the value of correlation dimension for the events mentioned above. The calculation procedure included standard steps (Theiler 1990a; Abarbanel et al. 1993; Isliker & Benz 1994) of the preliminary data analysis with stationarity tests, the reconstruction of a multidimensional attractor from the scalar data, and the correlation dimension estimation in different embedding dimensions. In addition, we have developed an approach for the detailed error analysis in the estimation procedure of the correlation dimension that enabled us to optimize calculation parameters such as the length of time series and scaling interval. It is described in the Appendix A and it is of particular interest not only for the processing of the solar emission data, but also for other applications.

Every case, where we detected saturation in the plot of the correlation dimension vs. embedding dimension, has been in-

spected by additional procedures to avoid false finite values of ν . It has been found that, like in many other works dealing with experimental data, the direct application of the procedure described often leads to spurious results. For example, in Fig. 2a,b we show the plots with clear saturation of the local slope curves. These plots have been obtained from the time interval indicated by arrows in Fig. 1c. In this case the saturation disappears after applying the surrogate or the shuffle data test (Theiler 1990a). However, we suppose that this saturation is solely defined by non uniformity of the reconstructed object which originates from the intermittency-like character of the time series investigated. This effect is illustrated in Fig. 1d, e, where two enlarged fragments of the processed interval, taken from its first and second halves, respectively, are shown. It is clear that the fragment in Fig. 1d contains temporal structures with much shorter characteristic periods than the one of Fig. 1e. As the process of reconstructing

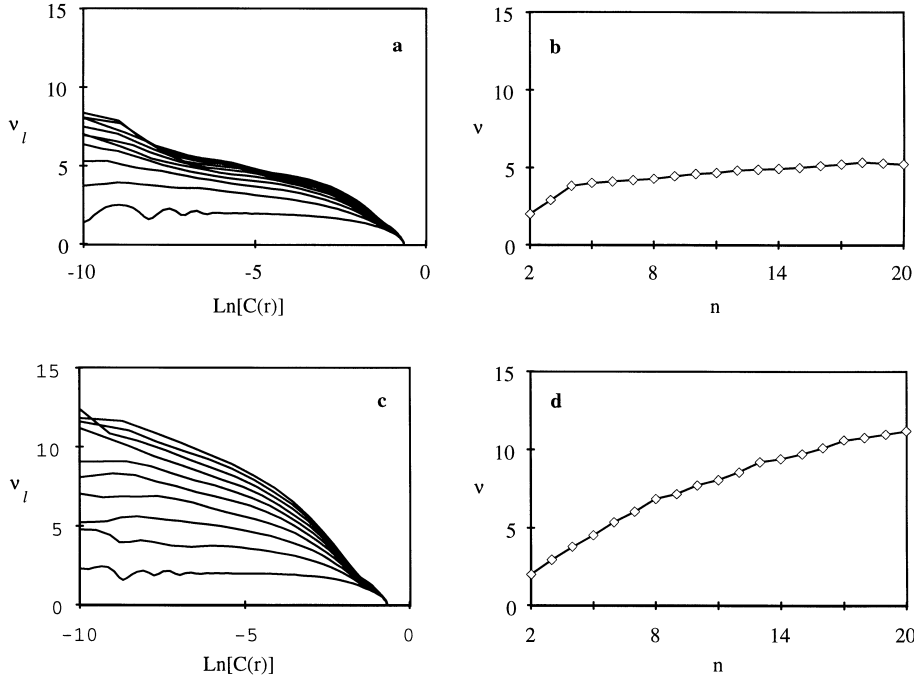


Fig. 2a-d. Analysis of the fragment from November 17, 1991 indicated by arrows in Fig. 1c: **a** and **c** Local slope $\frac{d(\ln C_n(r))}{d(\ln r)}$ vs. $\ln[C_n(r)]$ for $n = 2, 4, \dots, 20$, **b** and **d** correlation dimension ν_n vs. embedding dimension n . Whole fragment (a,b) and the first half of it (c,d).

the attractor by the method of delays with subsequent correlation dimension analysis is crucially dependent upon the time delay, and the optimal value of the delay time, in its turn, is defined by characteristic time scales of the investigated signal, the dominance of different time scales at different subintervals may lead to significant systematic errors in the final estimates of the dimension. This point is confirmed by the fact that after removal of the second half of the time interval from consideration the saturation disappears, as shown in Fig. 2c,d. So, we come to the conclusion that, for the time series investigated, there is no evidence of the presence of chaotic dynamics with dimension less than 10. The limiting value about 10 is defined by the length of time series used in our experiments (see Appendix A and Nerenberg & Essex 1990).

Although our results are consistent with those obtained by other authors for different wave bands, we would like to note that the question about the presence of chaos in the processes responsible for the millisecond pulsations is not closed yet. Some fundamental problems, still existing in the field of correlation dimension analysis, such as, for instance, the absence of clear ideas on how to obtain time series from experimental data which adequately describe the spatially extended burst-process or the influence of filtration usually performed in the receiver, do not allow to make a final conclusion about the dynamic properties of the studied signals. We now postpone this discussion until Sect. 6.

4. 1/f processes in the solar emission

In order to get additional information about the nature of the events studied, we exploit the recently proposed technique of signal processing based on the notion of wavelets. This approach is used for accepting or rejecting the hypothesis that the mea-

sured time profiles of the solar emission can be considered as a 1/f process with a background of white noise. Thus, we assume that the recorded signal $S(t)$ is approximated by

$$S(t) = f(t) + w(t). \quad (1a)$$

$$F(\omega) \propto \sigma_f^2 / \omega^\gamma \quad (1b)$$

Here $f(t)$ is a flicker-type process with the power spectrum approximated by the function (1b), σ_f is the standard deviation of this component, and γ is the spectral exponent, $w(t)$ is white Gaussian noise with the dispersion σ_w^2 . It is important to note that Eq. (1b) actually defines the magnitude of σ_f , which is not the infinite variance of the 1/f process, but the value extracted from the data, with the frequency spectrum confined within a definite interval. So defined, σ_f is dependent upon the time step and duration of the time series used, and is finite. Such a way of treating 1/f signals is commonly accepted and directly follows from their definition as the processes whose empirical power spectrum has the form (1b) in a wide frequency range.

The problem thus consists in extracting the parameters γ , σ_f , and σ_w from the data. We use for this purpose the variant of the maximum likelihood estimation for wavelet coefficients proposed by Wornell & Oppenheim (1992). The details of the calculation procedure are given in the Appendix B. The algorithm used turned out to be a robust one with respect to such parameters as the length of time series, the starting time of the analyzed fragment, and the intensity of the background noise.

An example of our calculations is depicted in Fig. 3. It contains the time profile and dependencies of the index γ and the signal to noise ratio ($\text{SNR} = \sigma_f^2 / \sigma_w^2$) upon time. Since the studied data are essentially non stationary, we estimated the value of γ over N -point segments of different duration ($N = 2^{11}, 2^{12}, 2^{13}$). By moving such segments along the realization or increasing

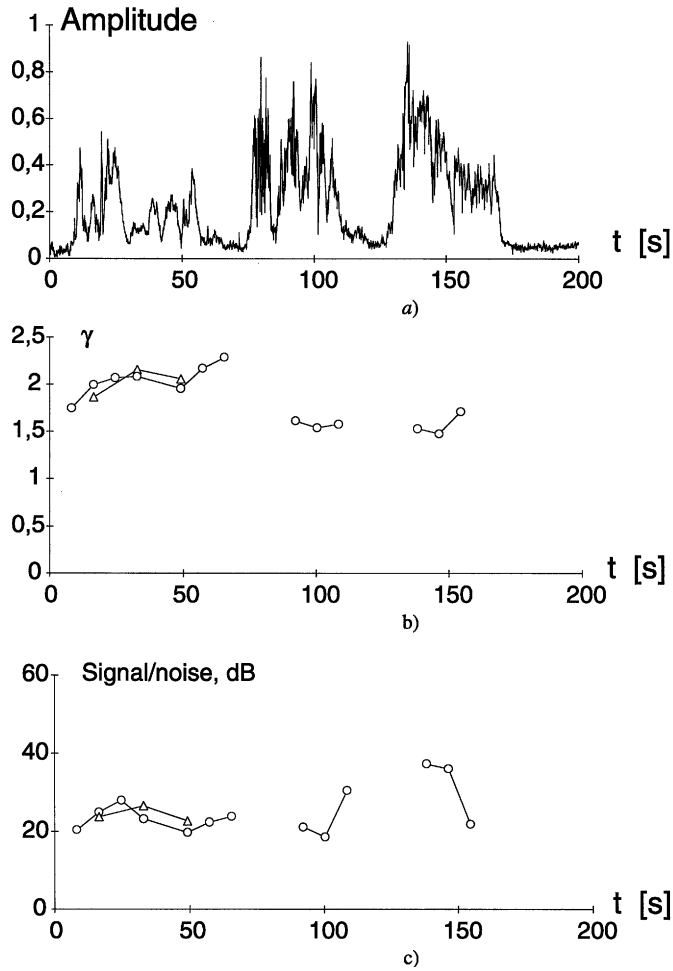


Fig. 3. **a** Time profile of a solar burst of November 17, 1991, at the frequency 2.85 GHz. **b** Value of the index γ vs. time. Points correspond to the centers of analyzed segments: Δ 4096 points, \circ 2048 points. **c** Values of the signal to noise ratio.

their length, we obtain the dependencies of γ on time or the length of the time interval. Then, we find the intervals in these dependencies where the r.m.s. deviation of γ (herefrom σ_γ) is less than 10% of the mean value of γ ; i.e. the regions with stable estimate of γ with respect to dilations or translations. We accepted this as a test of stationarity of the intervals and consider the value of σ_γ as a satisfactory estimate of the error of γ during the given part of a burst. Within the stationary parts of studied realizations we have also detected rather high value of SNR that enabled us to conclude that the proposed idealized $1/f$ model is an effective one for approximating the data.

The time profile in Fig. 3 has “quiet intervals” where the intensity of the emission is around the background noise level. When the flicker component is absent this manifests itself either as the lack of convergence of the γ estimation algorithm, or the obtained value of γ is accompanied by a low level of SNR. This explains the presence of discontinuities in the plot of γ vs. time.

The comparison of the plots obtained at different frequencies reveals a good correlation of the estimated values of γ for these

time series. It is worth noting that the SNR is somewhat higher at the frequency 2.85 GHz, that is a technical effect resulting from different noise levels in the recording channels of the measuring device. Thus, in such a manner, the procedure described may be also used for the calibration of equipment.

Thus, the results given above provide a strong evidence that the so-called millisecond pulsations in the solar emission belong to the class of $1/f^\gamma$ signals. The typical value of γ obtained in our numerical experiments approximately belongs to the interval [1; 2]. It is necessary to note, that in some cases the calculated value of γ was much less than 1, say about 0.5. However, in these occasions the magnitude of SNR was found to be much lower, compared to the results shown in Fig. 3, which did not allow us to interpret the data as $1/f$ signals.

To illustrate the quality of the $1/f$ model used, we plot in Fig. 4a the power spectrum of a part of the time profile shown in Fig. 3, together with the calculated linear fit line. One can see reasonably good agreement between both curves. In Fig. 4b,c we show also an example in the time domain, where the case (b) corresponds to the raw data, whereas (c) is the $1/f^\gamma$ part of the time series.

The application of the wavelet technique permits also to perform an effective filtration of the background white noise. The procedure is based on the calculation of wavelet coefficients \hat{f}_n^m of the $1/f$ process from the estimated values of dispersions $\hat{\sigma}^2$, $\hat{\sigma}_w^2$ and the exponent $\hat{\gamma}$ by using the formula (see Appendix B)

$$\hat{f}_n^m = \frac{\hat{\sigma}^2 2^{\hat{\gamma}m}}{\hat{\sigma}^2 2^{\hat{\gamma}m} + \hat{\sigma}_w^2} s_n^m$$

where s_n^m are wavelet coefficients derived from the application of the direct wavelet transform to the initial data. Then, using the inverse transformation we obtain the $1/f$ signal almost without the noise component. An example of the application of such a procedure is shown in Fig. 4, where the original data are compared to the filtered time series.

5. Pulse model of $1/f$ processes

The above calculations enable us to make two definite conclusions. First, pulsations of the solar emission during radio bursts, recorded with millisecond time resolution, can be approximated by $1/f^\gamma$ processes with typical values of $\gamma \in [1; 2]$. Second, the hypothesis about the low-dimensional deterministic origin of such processes, as follows from the correlation dimension analysis, can be rejected. The question naturally arises about the model capable of producing $1/f^\gamma$ spectra. We suppose that a train of random pulses

$$\xi(t) = \sum_{k=1}^N a_k F(t - t_k) \quad (2)$$

may be considered as a good candidate for the modeling of the observed signals. Here a_k and t_k are amplitudes and occurrence times of the pulses, considered to be independent random variables, $F(\cdot)$ is the shape of an individual pulse. It is well known

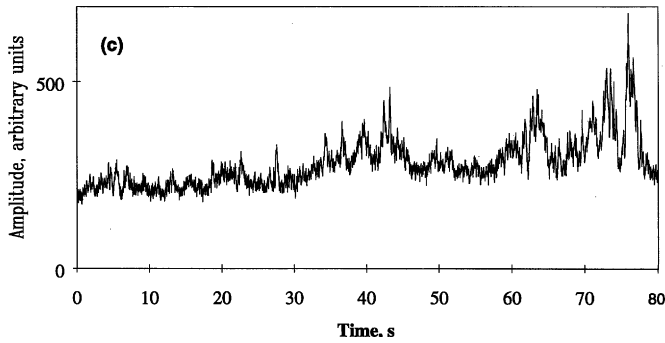
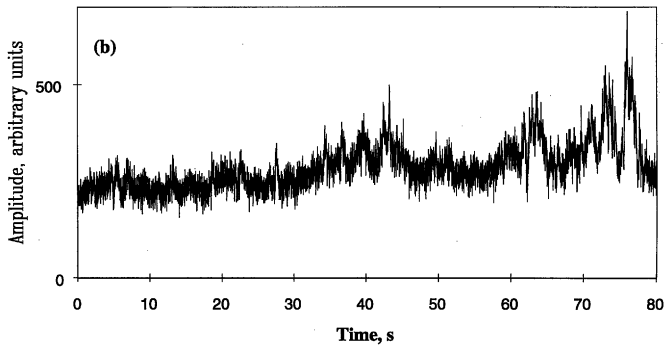
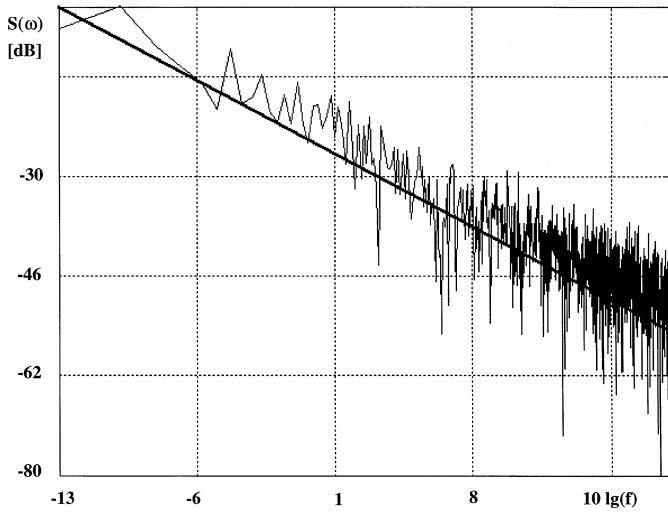


Fig. 4a–c. Quality of the fit of $1/f^\gamma$ model: **a** Power spectrum of a part of the fragment shown in Fig. 3 together with the linear approximation. **b,c** Fragment of the event No.6 from Table 1 at the frequency 2.5 GHz: **b** original data, **c** filtered component.

that under rather general assumptions concerning the distribution functions of a_k and t_k and suitable choice of the function $F(\cdot)$, the process (2) belongs to the class of $1/f^\gamma$ noises (Rytov 1966) at intermediate and high frequencies. From the other hand, the pulse-type model of the solar emission is one of the most frequently discussed in the literature (Islaker 1996; Islaker & Benz 1994; Barrow et al. 1994; Güdel & Benz 1990). In particular, the direct measurements of the shape of individual spikes in the frequency range 0.5–1 GHz demonstrate that they are indeed pulses, with fast front and much slower exponen-

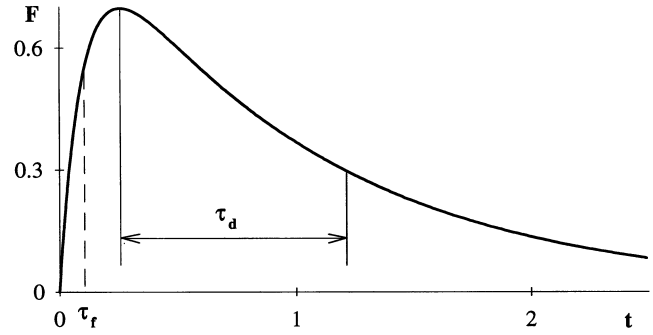


Fig. 5. Typical shape of an individual pulse for $\beta = 10$, $\alpha = 1$.

tial decay (Güdel & Benz 1990). The parameters defining the shape of pulses can be determined directly if their characteristic repetition time τ_r is greater than the pulse duration τ_p . However, if a different situation is met, i.e. the pulses overlap, that is presumably the case for our data, then it appears impossible to measure the characteristic times of the pulses by using conventional techniques.

Several approaches have currently been discussed for explaining the origin of pulsed structures in the solar emission. The pulsed radiation may appear, for example, due to the pulsed character of the injection of electrons into the solar magnetosphere. The generation of electron bunches may be related, in its turn, to the sudden rupture of electric current filaments in magnetic arches, resulting in the acceleration of groups of electrons (Parker 1979; Alfvén, 1981).

If to accept the process (2) as a working model, one can obtain some characteristic statistical properties of the pulsed emission, such as the time scale of pulse duration, the average repetition time, and the typical pulse amplitude. To determine these parameters in the solar emission we have carried out a series of numerical experiments with computer generated sequences of pulses of various shapes and characteristic times. We use the wavelet transformation with subsequent maximum likelihood estimation of the spectral index γ for the comparison of the artificial time series with actual data. The model used has the evident advantage of giving the possibility to analytically calculate the main characteristics of the resulting process of type (2).

It is easy to show that processes with $\gamma \leq 2$ arise if each pulse from the sequence (2) has, for example, the shape shown in Fig. 5. It is characterized by the presence of two significantly different time scales, the pulse front duration τ_f and decay time τ_d . We accept the following approximation for the pulse shape

$$F(t - t_k) = e^{-\alpha(t-t_k)} - e^{-\beta(t-t_k)} \quad (3)$$

with $\beta \gg \alpha$. It is characterized by two parameters: pulse raise time $\tau_f \approx 1/\beta$, and decay time $\tau_d \approx \tau_p \approx 1/\alpha$. As our calculations show, the specific functional form used for approximating the actual pulse shape is not critical for the determination of

physical parameters of the events. It is easy to show (Rytov 1966) that the power spectrum of the process (2) is given by

$$S(\omega) = 2\pi n \overline{|a|^2} \frac{(\beta - \alpha)^2}{(\alpha^2 + \omega^2)(\beta^2 + \omega^2)} \quad (4)$$

where n is the number of pulses per unit time (repetition frequency), $\overline{|a|^2}$ is the mean square amplitude of the pulses. Note, that the frequency dependence in (4) is solely defined by the power spectrum of an individual pulse of the form (3). For the subsequent analysis we need also the mean value of the process (2) and its dispersion

$$\overline{\xi(t)} = n\bar{a} \frac{\beta - \alpha}{\alpha\beta} \quad D(\xi) = \frac{\overline{|a|^2}}{n\alpha^2} \frac{(\beta - \alpha)^2}{2\alpha\beta(\alpha + \beta)} \quad (5)$$

where \bar{a} is the mean value of the pulse amplitude. In Fig. 6 the examples of realizations generated numerically in accordance with (2), (3) are given for the cases i) $\tau_r > \tau_p$ and ii) $\tau_r \ll \tau_p$. In our computer experiments we controlled the pulse repetition time τ_r by fixing the total observation time T and changing the number of generated pulses N_p . The amplitude of pulses is put equal to unity, and the occurrence times for each of them are random variables uniformly distributed over the interval $[0; T]$. It is clear that in the case i) corresponding to Fig. 6a it is possible to determine the characteristic time scales of an individual pulse, whereas for the second situation ii) all the time scales present in the realization are solely defined by the statistical properties of the whole sequence of pulses, and individual pulses are visually unresolved.

In our numerical experiments with solar data the value of γ was as a rule within the interval $[1, 2]$. However, one can note that there are different scaling regions in the power spectrum (4). The first one is defined by the condition $\omega \ll \alpha$, where $S(\omega) \approx \text{const}$ and $\gamma \approx 0$. The second subinterval is given by $\alpha \ll \omega \ll \beta$, where $S(\omega) \propto \omega^{-2}$, with $\gamma \approx 2$, and the third one where $\omega \gg \beta$ and $\gamma \approx 4$. It is evident, that if, for example, $\alpha \leq 2\pi/T$ and $\beta \geq 2\pi/t_s$, where t_s is the sampling time, then the value of γ is approximately equal to 2. So, we can obtain close to 2 magnitude of γ if the frequency interval of our calculation is

$$\alpha < \frac{2\pi}{T} \equiv \omega_1 \leq \omega \leq \omega_2 \equiv \frac{2\pi}{t_s} < \beta. \quad (6)$$

To illustrate the interplay between these characteristic time scales we plot in Fig. 7a schematic of the power spectrum (4) where three characteristic regions are clearly seen, along with the frequency interval of our study.

We are now in a position to calculate α , together with other characteristics, such as the repetition time and the mean value of the amplitude of pulses. We start by noting that we have never observed a clear characteristic ‘‘knee’’ in the high-frequency part of the power spectrum similar to that shown in Fig. 7 in any of the power spectra obtained from the experimental data. This means that the value of β lies outside the detectable frequency range in our experiments, and we can put $\beta = \infty$ without introducing any additional errors. Such a conclusion enables us to get

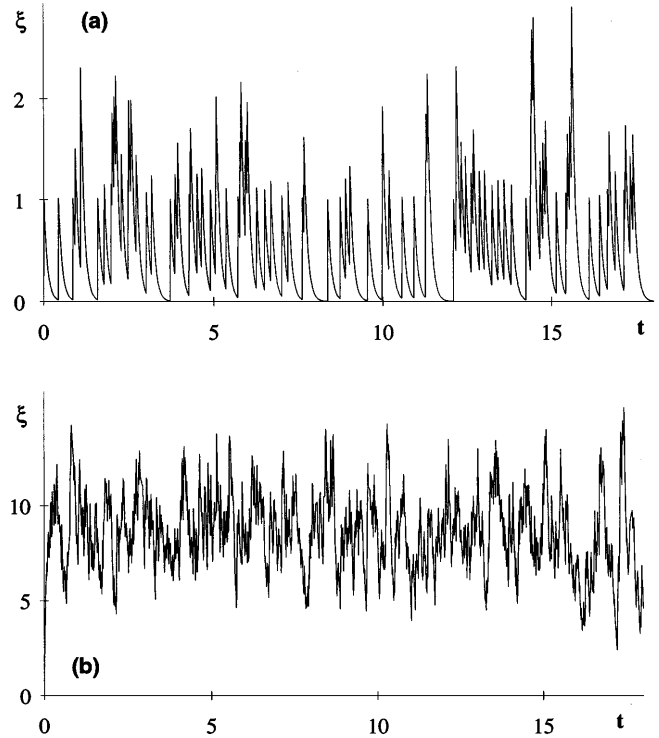


Fig. 6a and b. Numerically generated time series at $\beta = \infty$ and $\alpha = 10(\tau_p = 0.1)$: **a** repetition time $\tau_r = 0.2$, **b** $\tau_r = 0.0125$.

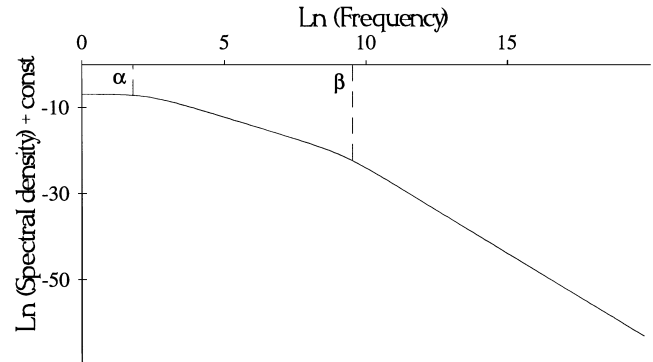


Fig. 7. Power spectrum of the process defined by (2), (3) at $\alpha = 10$, $\beta = 10^4$.

a one to one correspondence between the value of γ extracted directly from experimental data, by means of the wavelet transform plus maximum likelihood techniques, and the parameter α defining the shape of an individual pulse. For this purpose, we have performed a series of numerical experiments with random sequences of pulses of equal amplitude and various values of α and n . These numerically generated time series have been processed by the above technique, and for various α and $N_p \equiv nT$ the magnitude of γ has been calculated. It has been found that γ is only slightly dependent on N_p if $N_p \geq 100$ (which was always the case for the processed observational data). The resulting curve is shown in Fig. 8, where we plot the dependency averaged over hundreds of different pulse sequences. So, we

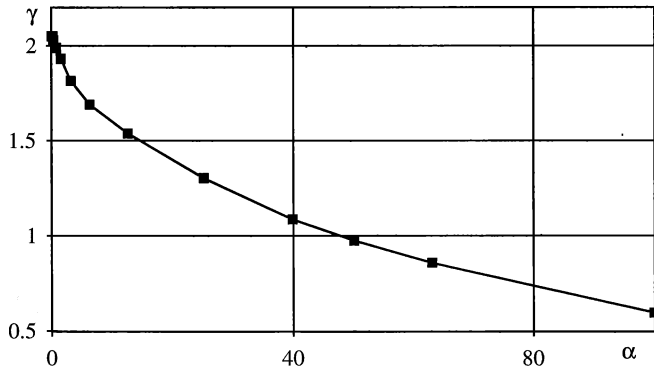


Fig. 8. Reference curve for finding α values by calculated magnitudes of γ .

can obtain the value of α by the calculated magnitude of γ by using the plot of Fig. 8 as a reference curve.

When getting the α – γ plot, we neglect the possible variation in amplitudes a_k and consider the process of the type (2) with pulses of equal amplitude. This allows us to put $\overline{a^2} = \bar{a}^2$ which introduces not significant error compared to the case of a more realistic assumption on a_k distributed in accordance with the Rayleigh distribution when

$$\frac{\overline{a^2}}{\bar{a}^2} = \frac{4}{\pi}$$

that is not considerably different from unity.

Now let us calculate other characteristics of pulse sequences, such as the average repetition time and the mean amplitude. We make use of the expressions for the mathematical expectation and dispersion of (5) which are for $\beta \gg \alpha$

$$\overline{\xi(t)} = \frac{n\bar{a}}{\alpha}; \quad D(\xi) = \frac{n\bar{a}^2}{2\alpha}. \quad (7)$$

Combining (7) with the value of α derived from Fig. 8 we obtain the algebraic equations relating n and \bar{a} to the values of $\overline{\xi(t)}$, $D(\xi)$ and α which can be directly calculated from the experimental data and the calibration curve of Fig. 8.

$$\bar{a} = 2 \frac{D(\xi)}{\overline{\xi(t)}}; \quad n = \frac{\alpha \overline{\xi(t)}^2}{2D(\xi)}. \quad (8)$$

With the help of (8) and Fig. 8 we have carried out the calculation for solar radio emission data. The results are summarized in the Table 2 where the pulse durations have been calculated as the inverse of α values found from Fig. 8.

Let us now dwell upon some major regularities in the calculation results. The pulse durations, equal to the characteristic decay time $1/\alpha$, range from 13 to 500 ms. So, some of the studied events (the first six in Table 2) are in rather good agreement with the results reported by Güdel & Benz (1990). The remaining ones have much longer duration. If one assumes that the pulsed emission is produced by bunches of electrons moving in the solar corona, then these time intervals may be associated either with the lifetime of an individual bunch or the time of

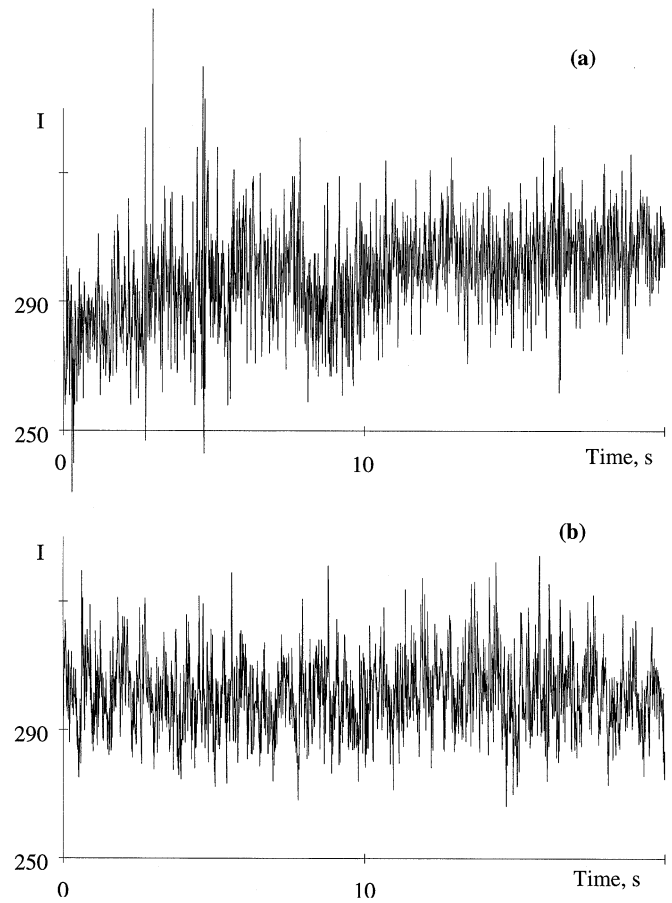


Fig. 9 a and b. Intensity (arbitrary units) vs. time for original and corresponding artificial time series. Event No. 2 from Table 1: **a** original, **b** artificial.

radiation to the direction of the Earth observer. The variation of the repetition time is also rather high, from 500 to 0.1 ms, which corresponds to the repetition frequency from 2 to 8000 Hz.

As the duration of an individual pulse is as a rule greater than the repetition time, the observed variability in the time series studied is mainly determined by the statistical effect of superposition of many stochastically generated pulses. Thus, the time series typically possess time scales which are not directly related to the characteristic times of pulsed emission. In particular, the millisecond pulsations, intensively discussed in the literature, may be solely the manifestation of the statistical properties of the overlap of several pulses.

In the present work we have not analyzed in detail the accuracy of the estimates obtained for \bar{a} and n . We performed only a series of numerical tests to roughly evaluate the associated errors. For every set of parameters found from the data processing we generated some tens of artificial sequences of pulses with the same parameters. As one can expect, the error values turn out to be strongly dependent upon the magnitude of n , and the error grows with decreasing n . For example, for $n < 10$, the error is typically larger than 50%. So, in such cases, the obtained values of parameters indicate only their orders of magnitude.

Table 2.

Number of an event (see, Table 1)	Frequency GHz	Initial point	Number of points	γ	SNR, dB	α_γ	τ_p , ms	\bar{a} , SFU	n, pulse/ second
2	2.5	900	4096	0.9	31.3	58	17	3.1	5524
2	2.85	900	4096	1.1	27.7	40	25	1.18	7945
5	2.5	9000	4096	1.1	26.0	40	25	29.5	390
5	2.85	9000	4096	1.4	14.2	20	50	109.0	403
5	2.5	9500	1024	1.1	32.4	40	25	33.2	320
5	2.85	9500	1024	0.8	26.8	75	13	73.2	243
5	2.5	1000	2048	1.9	20.2	2	500	97.6	3.3
6	2.5	0	8192	1.7	9.2	6	167	94.7	5.0
6	2.85	0	8192	1.8	14.6	3.5	286	51.4	2.2
7	2.5	900	4096	1.8	12.1	3.5	286	68.1	4.2

Additional support for our model of the solar emission is given by the numerically generated realizations given in Fig. 9. Here we plot some of the studied events together with the simulated time series at the identical values of parameters defining the pulse shapes and repetition times. Some additive noise has been added, to keep the signal to noise ratio equal to the value extracted from the raw data by means of wavelet analysis. In our view, there is reasonably good agreement between the overall appearance of the artificial and original data.

6. Discussion and conclusions

There are several fairly independent results in the paper which may be considered as approximations of real events on the Sun to different extents. First, we have demonstrated that the studied mcw-bursts at frequencies 2.5 and 2.85 GHz are not of low-dimensional deterministic nature. We can interpret this result as an additional confirmation of some similar conclusions of other authors (Isliker & Benz 1994). At the same time, we think that the question of deterministically chaotic vs. stochastic origin of the measured time series from the solar radiation is not yet closed. In the calculation procedure of the correlation dimension, there are several so far unsolved problems which turn out to be crucial for the final conclusions. For example, the issue of filtration of the data in the process of a measurement should be mentioned. It is clear that the filtration, together with a nonlinear transformation (say, in detector) may result in an essential increase in the estimated dimension value, to the extent where the deterministic signal can not be distinguished from stochastic noise. This problem is closely related to another one, still existing in the application of the correlation dimension analysis to the investigation of spatially variable phenomena, like solar flares, for example. Usually, the measurements of the radio flux from the Sun are performed within a definite frequency band, as the behavior at different frequencies is associated with processes in spatially separated regions. It remains unclear how to construct properly the time series for the correlation dimension analysis. Whether it should be the output of the detector of a narrow band receiver, or the frequency band taken into account must be as wide as possible in order to include all spatial varia-

tions, or a “natural” frequency range associated with the given phenomenon, has to be investigated.

Another result of the paper consists in the detection of a $1/f^\gamma$ component in the emission. It is obtained via the well-defined and justified technique based on wavelet transformation and maximum likelihood estimation. It is important that the intensity of $1/f^\gamma$ signal has been found to be much higher than the background white noise. The high signal to noise ratio enables us to make conclusions on the reliability of this result. At the same time, we would like to note that $1/f^\gamma$ spectral component is present only approximately, and only within an intermediate frequency range defined by the time resolution of the experimental setup from the side of high frequencies and the finite duration of observed events from the low frequency one. It should also be mentioned that the presence of $1/f^\gamma$ process in the cases studied does not imply that the only possibility for their origin is a stochastic noise. Chaotic oscillations can also lead to the $1/f^\gamma$ spectral behavior, as it has been shown by Ben-Mizrachi et al. (1985) or Arecchi & Califano (1987). In such case, the mechanism producing the $1/f^\gamma$ shape of the spectrum may be attributed to intermittency.

We have suggested a pulsed model of the solar emission during mcw-bursts which satisfactorily reproduces $1/f^\gamma$ properties of the measured signals for a specific choice of the shape of an individual pulse. Such a description is, of course, not a unique explanation for the $1/f^\gamma$ character of the measured power spectrum and gives only a statistical approximation to the observed time profiles. The motivation for our approach comes from two main considerations. First, $1/f^\gamma$ processes arise as a result of the superposition of pulses in many physical situations (van der Ziel 1979). Second, the conjecture about the pulsed nature of solar mcw-emission has been put forward independently in many other works. Our contribution to this field consists in the procedure developed for extracting the parameters of pulses from the raw data. The principal difficulty in such kind of a study is that characteristic time scales of pulses are hidden because of the substantial overlap of pulses. It is interesting that due to the statistical character of the process of pulses generation, almost any time scale appears to be present in the data. Because of this, the separation of millisecond time scales is not well defined since

they are not distinguishable from other time scales present in the data.

The proposed pulsed model also permits one to describe self consistently the build-up process of the bursts, without making any additional assumptions about the mechanisms underlying the initial stage of burst development. In the framework of our approach, the gradual increase in the mean intensity is mainly determined by the process of pulses accumulation. That is why the process of pulse generation starts before the stationary part in the observed realizations. Along with the pulse duration τ_p , which is assumed to be equal to the decay time, there are two other time scales, the repetition time τ_r and the rise time of the pulse τ_f . Our approach gives satisfactory estimates for τ_p and τ_r , but does not allow us to extract the rise time. So far, only a very rough estimate of τ_f is possible which comes simply from the sampling rate of the measurement. It is clear that in our model β should be much greater than α , which means that the typical shape of a pulse is defined by the fast increase and slow decay phases. Such a shape is consistent with the results of direct measurements performed by Güdel & Benz (1990) in another frequency band.

The model is also consistent with some of the physical mechanisms of burst generation discussed in the literature. It is now commonly accepted that the pulsed character of the emission is related to the particle acceleration in magnetic fields generated by electric currents in the solar corona. At the same time, the physical conditions in the emitting region are not well understood. A frequently discussed mechanism is the sudden disruption of electric current filaments due to plasma instabilities. Another possibilities are pulsed injection of electron beams into the coronal arches, synchronized by magneto hydrodynamic oscillations or nonlinear relaxation oscillations due to wave-particle interactions. We suppose that the results of our study can be used in a detailed analysis of some of these mechanisms.

We would also like to note the apparent similarity in $1/f^\gamma$ spectral behavior of the studied events with the pulsations of solar emission of the noise-storm type (Takakura 1959). This shows that the decimeter and meter pulsations may have similar properties in spite of considerable differences in characteristic time scales: decimeter pulsations arise during bursts and last for about 1 minute, whereas noise storms occur in meter waveband and have the duration of the order of some weeks, without any clear relation to flares.

Acknowledgements. V.B. Ryabov acknowledges support from INTAS (contract INTAS-94-1296) and NATO Science Fellowship. This research was also supported by the International Science Foundation (grant # U33000). We thank Dr. H. Isliker for a critical reading of the paper resulted in a substantial improvement of the article, and Prof. P. Robinson for his helpful comments.

Appendix A: hypercube model and errors of calculations

To evaluate the accuracy of correlation dimension estimates, the n -dimensional hypercube model is commonly used. It is assumed in the framework of this model that N points are uniformly distributed (in the sense of constant probability density)

over a n -dimensional unit cube. Such an approach permits one to obtain the estimate for two kinds of errors, namely, the systematic bias defined by boundary effects and random uncertainties originating from the finiteness of the number of points N . Although such a model does not take into account a nonuniformity in the distribution of points, which is always the case in any calculation, it gives a sufficiently exact estimate in the spaces of dimension less than the correlation dimension of the explored signal.

The correlation dimension ν was introduced as an exponent in the power law (Grassberger & Procaccia 1983)

$$C_n(r) \sim r^\nu$$

as $r \rightarrow 0$, where $C_n(r)$ is the correlation integral in the n -dimensional space. For the initial data set, the experimental time series (signal record) in the form of M discrete scalar points $\{x_i\}$ ($i = 1, 2, \dots, M$), sampled with the time interval Δt_s , is usually considered. Then, the reconstruction of the n -dimensional vector signal Y_k from the scalar data $\{x_i\}$ is performed. As a result, the set of $N = M - mn - 1$ points is defined in the n -dimensional space where m is an integer. The Packard-Takens procedure is usually used for such a reconstruction, utilizing the time-delayed x values as the components of an n -dimensional vector Y_k , with the time delay $\tau = m\Delta t_s$

$$Y_k = (x_k; x_{k+m}; \dots; x_{k+(n-1)m}), \quad k = 1, 2, \dots, N$$

When the process is generated by a dynamical system with small number of degrees of freedom, the reconstructed object is topologically equivalent (in the sense of equality of fractal dimension) to the attractor of this system.

The calculation of correlation integrals is subsequently performed in accordance with the formula

$$C_n(r) = \frac{1}{n_0} \sum_{i=1}^{N-q-1} \sum_{j=i+1+q}^N \theta(r - \|Y_i - Y_j\|)$$

where $\theta(\cdot)$ is the Heaviside function, $n_0 \approx N^2$ is the number of interpoint distances, q is the integer defining the minimal time separation between points (Theiler, 1990a), $\|\cdot\|$ the norm in the n -dimensional space in the general case defined by

$$\|Y_i - Y_j\| = \left[\sum_{k=1}^n |y_{ik} - y_{jk}|^\gamma \right]^{1/\gamma}$$

where γ is a positive number, y_{ik} is the k -th coordinate of the i -th point. The case of $\gamma = 2$ corresponds to the usual Euclidean distance. ν_n value is estimated as the slope of a straight line in the coordinates $\log[C_n(r)] - \log(r)$.

$$\nu_n(r) = \frac{d[\ln C_n(r)]}{d[\ln(r)]}; \quad \nu = \lim_{r \rightarrow 0} \lim_{n \rightarrow \infty} \nu_n(r)$$

By definition, the correlation integral is the probability distribution function for interpoint distances. If one assumes the

statistical independence of all the n_0 distances, then the magnitude of the error in the estimate of correlation integral can be derived from the fact that the calculated value $C_n^*(r_0)$ for arbitrary r_0 is a random variable with the binomial distribution defined by its mathematical expectation $C_n(r_0)$ and dispersion $D = C_n(r_0)[1 - C_n(r_0)]/n_0$. If $Dn_0^2 \geq 9$, the binomial distribution can be well approximated by the Gaussian one with the same parameters. This permits one to find the confidence interval $[C_n^{(1)}, C_n^{(2)}]$ that covers the value obtained $C_n^*(r_0)$ with a probability P_C :

$$C_n^{(1,2)} = \frac{2n_0 C_n^*(r_0) + t^2 \pm t \sqrt{4n_0 C_n^*(r_0)[1 - C_n^*(r_0)] + t^2}}{2(n_0 + t^2)} \quad (\text{A1})$$

The parameter t is defined by P_C and can be found in reference tables (e.g. at $t = 1$, $P_C = 0.68$; at $t = 2$, $P_C = 0.95$; etc.). As $N \gg 1$, the Eq. (A1) can be considerably simplified, and the approximate value of the absolute error in the correlation integral can be easily deduced and taken equal to the half of the confidence interval $[C_n^{(1)}, C_n^{(2)}]$

$$\Delta C_n^{(R)} \equiv \frac{C_n^{(2)} - C_n^{(1)}}{2} \approx \frac{t \sqrt{C_n^*(r_0)}}{n_0} \approx t \sqrt{\frac{C_n^*(r_0)}{N}} \quad (\text{A2})$$

As one could expect, the magnitude of the random error decreases as $1/N$ (Theiler 1990b). The relative error $\Delta C_n/C_n^*(r_0)$ increases with observational resolution.

To evaluate the systematic bias value let us make use of the expression for the correlation integral obtained by Litvinenko et al. (1992) for a hypercube

$$C_n(r) = r^n \sum_{k=0}^n a_{nk} r^k, \quad (r < 1)$$

$$a_{nk} = (-1)^k \frac{n!}{k!(n-K)!} \frac{2\pi^{(n-k)/2}}{(n+k)\Gamma((n+k)/2)}, \quad (\text{A3})$$

where $\Gamma(\cdot)$ is the gamma-function, and distances are assumed to be Euclidean. For the hypercube considered, the correlation dimension equals the space dimension n . In formula (A3) all terms in the sum beginning from $k = 1$ contribute to the error. Its magnitude grows with r and tends to zero as $r \rightarrow 0$, with

$$\Delta C_n^{(B)} = r^n \sum_{k=1}^n a_{nk} r^k. \quad (\text{A4})$$

Consider now how the errors in the correlation integral defined by Eqs. (A2), (A4) influence the ν_n value. For this purpose we take the following formula for the dimension estimate

$$\nu_n^* = \frac{\ln[C_n(r_2)] - \ln[C_n(r_1)]}{\ln r_2 - \ln r_1} \quad (\text{A5})$$

where r_1 , and r_2 are arbitrary. Since the exact value of ν_n is known and equals n , the magnitude of systematic bias can be estimated as $n - \nu_n^* \equiv \Delta_\nu^{(B)}$.

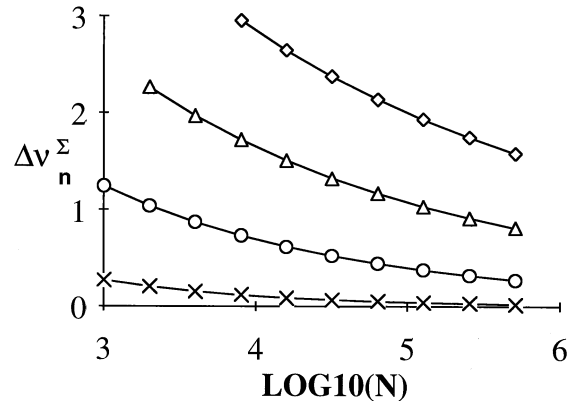


Fig. A1. Minimal error in ν_n estimate at $n = 3$ (crosses), 7 (circles), 11 (triangles), 15 (squares) for $t = 3$.

The contribution from random errors is defined by

$$\Delta_\nu^{(R)} = \frac{1}{\ln(r_2) - \ln(r_1)} \times \ln \frac{[C_n(r_2) + \Delta C_n^{(R)}(r_2)][C_n(r_1) + \Delta C_n^{(R)}(r_1)]}{[C_n(r_2) - \Delta C_n^{(R)}(r_2)][C_n(r_1) - \Delta C_n^{(R)}(r_1)]} \quad (\text{A6})$$

By virtue of the fact that, with a decrease in r_2 and r_1 , the random error grows and the systematic one decreases, there exist optimal values of r_2 and r_1 at which the total error $\Delta_\Sigma = \Delta_\nu^{(B)} + \Delta_\nu^{(R)}$ is minimal. In Fig. A1 the dependencies are given of the minimal total error Δ_Σ on the embedding space dimension n at different values of N .

It should be noted that the main contribution to the total error is made by the systematic bias, and it can reach significant values, making impossible the reliable detection of the deterministic signal with the dimension larger than 8–10 in the time series shorter than $10^5 - 10^6$. Moreover, the given above value of errors underestimates the uncertainty, and the restrictions on the length of time series may turn out to be much more substantial.

Appendix B: wavelet analysis and maximum likelihood estimation

The method of obtaining the estimate of the parameters γ , σ_f^2 , and σ_w^2 has been proposed by Wornell and Oppenheim and is based on the maximization of the maximum likelihood function for wavelet coefficients s_n^m of the signal (1). The coefficients are derived from the orthonormal discrete wavelet transformation.

The wavelet coefficients s_n^m of the process $s(t) \in L^2(R)$ are the projections of the function $s(t)$ to the full orthonormal basis $\varphi_n^m(t)$ in $L^2(R)$

$$s_n^m = \int_{-\infty}^{\infty} s(t) \varphi_n^m(t) dt. \quad (\text{B1})$$

The functions $\varphi_n^m(t)$ are called wavelets and possess the basic property of being derived from dilations and translations of one and the same basic wavelet $\varphi(t)$:

$$\varphi_n^m(t) = 2^{-m/2} \varphi(2^{-m}t - n) \quad (B2)$$

$$m, n \in \{\dots, -2, -1, 0, 1, 2, \dots\}'$$

where m is the scaling index, and n is the translation one. The function $\varphi(t)$ must satisfy certain conditions which are discussed in detail, for example, by Daubechies (1988). Since $\varphi_n^m(t)$ constitute a full basis in L^2 , the process $s(t)$ can be restored by its wavelet coefficients:

$$s(t) = \sum_m \sum_n s_n^m \varphi_n^m(t) \quad (B3)$$

So, the wavelet transformation performs the time-scale decomposition of the signal $s(t)$. Since we have a discrete and finite version of the signal $S(t)$ as an input for the processing, it is convenient to use the theory of multiple scale analysis (Mallat 1989) and discrete wavelet transformation algorithms (Mallat 1989; Rioul & Duhamel 1992) for the computation. To get the coefficients s_n^m in our work, we use the pyramidal algorithm (Mallat 1989) which is one of the most efficient numerical algorithms for the discrete wavelet transformation.

Because of the linearity of the wavelet transformation, the wavelet coefficients s_n^m for the process (1) are also the sum of two components

$$s_n^m = f_n^m + w_n^m \quad (B4)$$

If $f(t)$ is a 1/f process with the power spectrum of the form $S\omega \approx 1/\omega^\gamma$, the wavelet coefficients constitute a progression (Wornell 1990, 1991)

$$\text{Var}(f_n^m) = \sigma^2 2^{m\gamma}, \quad (B5)$$

where σ^2 is the constant, proportional to the signal variance σ_f^2 , and γ is the index of 1/f process. For the variance $\text{Var}(s_n^m) = \sigma_m^2$, we have

$$\sigma_m^2 = \sigma^2 2^{m\gamma} + \sigma_w^2 \quad (B6)$$

by taking (B5) and the mutual independence of the processes $f(t)$ and $w(t)$ in (1) into account. It is assumed that the wavelet coefficients f_n^m of the 1/f process are independent or have at most a small correlation in both indexes n and m (Wornell & Oppenheim 1992; Wornell 1990, 1991). Therefore, if to assume $f(t)$ and $w(t)$ in (1) to be Gaussian, the estimate of the unknown parameters σ^2 , γ , σ_w^2 in (B6) can be obtained by the maximum likelihood technique. The logarithmic likelihood function has the form (Wornell & Oppenheim, 1992)

$$L(s_n^m; \sigma^2, \gamma, \sigma_w^2) = -\frac{1}{2} \sum_m n(m) \frac{\hat{\sigma}_m^2}{\sigma_m^2} + \ln(2\pi\sigma_m^2) \quad (B7)$$

where $\hat{\sigma}_m^2 = \frac{1}{n(m)} \sum_n (s_n^m)^2$ are m calculated variances.

The numerical algorithm for the estimation of the maximum of the function (B7) may be found in (Wornell & Oppenheim, 1992), and it provides the estimates $\hat{\sigma}^2$, $\hat{\gamma}$, $\hat{\sigma}_w^2$ of the sought-for

parameters. The results obtained with the method of maximum likelihood are asymptotically stable and robust. The errors may be calculated from Fisher's information matrix, which also gives the lower limit for the variance of the estimates.

From $\hat{\sigma}^2$, $\hat{\gamma}$, $\hat{\sigma}_w^2$, the wavelet coefficients f_n^m of the 1/f process in (B4) can be found. By using the method of maximum likelihood we have the following estimate

$$\hat{f}_n^m = \frac{\hat{\sigma}^2 2^{-m\hat{\gamma}}}{\hat{\sigma}^2 2^{-m\hat{\gamma}} + \hat{\sigma}_w^2} s_n^m \quad (B8)$$

The Eq. (B8) gives the ratio of variance of wavelet coefficients of the 1/f process to the variance of the coefficients of the signal $s(t)$ at m -th step of approximation. It can be used for estimating the efficiency of approximating $s(t)$ with the flicker noise model, which is accomplished by calculating the signal to noise ratio, regarding $f(t)$ as the signal in (1). To obtain this estimate, we have to evaluate the variance σ_f^2 of the signal $f(t)$. It seems natural to use for this purpose the inverse discrete wavelet transformation of the coefficients (B14), which is a better way of getting the estimate for σ_f^2 than, for example, using the magnitude of $\hat{\sigma}^2$ which is proportional to σ_f^2 . It is not convenient to use $\hat{\sigma}^2$ for computing the σ_f^2 for two reasons. First, the exact relation between $\hat{\sigma}^2$ and σ_f^2 depends both on absolute values of an index m and on the shape of the wavelet function. Second, the maximum likelihood estimate $\hat{\sigma}^2$ is rather uncertain, due to the exponential dependence on γ in (B7).

References

- Abarbanel H.D.I., Brown R., Sidorowich J.J., Tsimring L.Sh., 1993, Rev. Mod. Phys. 65, 1331
- Alfvén H., 1981, Cosmic plasma. D.Reidel Publ. Co., Dordrecht, Holland
- Arecchi F.T., Califano A., 1987, Europhys. Lett. 3, 5
- Aschwanden M.J., 1987, Solar Phys. 111, 113
- Barrow C.H., Zarka P., Aubier M.G., 1994, A&A 286, 597
- Ben-Mizracchi A., Procaccia I., Rosenberg N., Schmidt A., 1985, Phys. Rev. A 31, 1830
- Benz A.O., Aschwanden M.J., 1991, Characteristics of the impulse phase of flares. In: Lecture Notes in Physics. IAU Coll., p.133
- Daubechies I., 1988, Commun. Pure Appl. Math. 41, 909.
- Dennis B.R., Orwig L.E., Kiplinger A.L. (eds.), 1987, Rapid fluctuations in solar flares. NASA Conf. Publ. NASA CP 2449. 1987
- Grassberger P., Procaccia I., 1983, Physica 9D, 189
- Güdel M., Benz A.O., 1990, A&A 231, 202.
- Islaker H., 1992, Solar Phys. 141, 325
- Islaker H., Benz A.O., 1994, A&A 285, 663
- Islaker H., 1996, A&A, 310, 672.
- Kurths J., Herzel H., 1987, Physica D 25, 165
- Kurths J., Karlicky M., 1989, Solar Phys. 119, 399
- Litvinenko L.N., Ryabov V.B., Usik P.V., Vavriv D.M., 1992, Correlation Dimension: The New Tool in Astrophysics. Preprint No.64, Institute of Radio Astronomy, Kharkov.
- Mallat S., 1989, IEEE Trans. Pattern Anal. Machine Intell. 11, 674.
- Nerenberg M.A.H., Essex C., 1990, Phys.Rev.A 42, 7065
- Parker E.N., 1979, Cosmical magnetic fields. Their origin and their activity. Clarendon press, Oxford.

- Rioul O., Duhamel P., 1992, IEEE Trans. on Information Theory 38, 111.
- Rytov S.M., 1966, Introduction to statistical radio physics (in Russian). Nauka, Moscow.
- Slottje C., 1978, Nat. 275, 520
- Stepanov A.V., Yurovsky Yu.F., 1990, Pis'ma v Astron. Zhurn. 16, 247
- Takakura T., 1959, Astr. Soc. of Japan 11, 55.
- Theiler J., 1990a, J. Opt. Soc. Am. A 7, 1055
- Theiler J., 1990b, Phys. Rev. A 41, 3038
- Vlahos L., Sharma R.R., Papadopoulos K., 1983, ApJ 275, 374
- Wornell G.W., Oppenheim A.V., 1992, IEEE Trans. of Signal Processing 40, 611.
- Wornell G.W., 1990, IEEE Trans. Information Theory 36, 859
- Wornell G.W., 1991, Synthesis, analysis, and processing of fractal signals. RLE Tech Rep.566, M.I.T., Cambridge, MA
- Zaitsev V.V., Stepanov A.V., Sterlin A.M., 1985, Sov. Astron. Lett. 11, 192
- van der Ziel A., 1979, Advances in Electronics and Electron Physics 49, 225